Applied Energy 248 (2019) 576–588

Contents lists available at ScienceDirect

Applied Energy

journal homepage: www.elsevier.com/locate/apenergy

Evaluation of the passive pre-chamber ignition concept for future high compression ratio turbocharged spark-ignition engines

J. Benajes[a], R. Novella[a,*], J. Gomez-Soriano[a], P.J. Martinez-Hernandiz[a], C. Libert[b], M. Dabiri[b]

[a] CMT – Motores Térmicos, Universitat Politécnica de Valéncia, Camino de Vera, 46022 Valencia, Spain
[b] DEA-IRP Groupe Renault, 1 avenue du Golf, 78084 Guyancourt, France

HIGHLIGHTS

- TJI concept was implemented in a high compression ratio turbocharged SI engine.
- A numerical methodology was developed to design pre-chambers geometry.
- Selected pre-chamber designs were experimentally evaluated and scored.
- TJI concept is unable to extend dilution ratio to avoid the use of TWC system.
- TJI concept is less tolerant to EGR dilution than the standard ignition concept.

ARTICLE INFO

Keywords:
Spark-ignition engine
Pre-chamber ignition
Lean burn
EGR dilution
Efficiency and emissions

ABSTRACT

The pre-chamber ignition concept is an attractive strategy to enable the operation of spark-ignition engines in lean or diluted conditions keeping a suitable combustion process. According to the results the benefits in lean conditions include the combustion process shortening, the improvement of combustion stability and the increase of combustion efficiency by lowering carbon monoxide and hydrocarbons emissions. Thus, the pre-chamber ignition concept, especially in its passive version, arises as a promising alternative for future spark-ignition engines for passenger car applications. In this framework, an experimental investigation has been carried out to evaluate the potential of passive pre-chamber ignition concept in a high compression ratio, turbocharged, port fueled spark-ignition engine, using 95 Research Octane Number gasoline. As a first step, a 1D Wave Action Model was generated to design the pre-chamber geometry taking the fuel available at the start of pre-chamber combustion and the pressure difference between the main chamber and pre-chamber as key parameters. In a second step, these pre-chamber designs were experimentally validated at high load/speed conditions (4500 rpm, 12.5 bar Indicated Mean Effective Pressure) and compared with the conventional spark-ignition concept. Experimental results show how the passive pre-chamber concept increases efficiency with good combustion stability and high combustion efficiency in stoichiometric conditions. Nevertheless, maximum lambda attainable with the passive system is similar than that of the conventional spark and much lower compared to the maximum levels reported for the active system.

1. Introduction

During the last years there has been a trend shift in the passenger car sales at the European market due to different social, political and economic aspects. The compression-ignition (CI) powerplant sales fell down and its main competitor, the spark-ignition (SI) powerplant, has taken up the market share left. The extracost associated to the CI engine related hardware required to fulfil the extremely restrictive European emissions standards is probably the most important factor [1]. However, SI engines provide worse efficiency and then fuel economy figures compared to the equivalent CI engines [2]. The main reasons are the low compression ratio (between 8:1 and 12:1) and the necessity to operate the engine in a stoichiometric air-to-fuel ratio ($\lambda = 1$). The octane number of the fuel and the intrinsic engine knock tendency determine the compression ratio limit, both aspects widely investigated by other authors [3]. The stoichiometric air-to-fuel ratio limitation is related to the necessity to keep an adequate flame propagation velocity to keep a suitable combustion performance [4] and the use of the three-

* Corresponding author.
E-mail address: rinoro@mot.upv.es (R. Novella).

https://doi.org/10.1016/j.apenergy.2019.04.131
Received 21 February 2019; Received in revised form 26 March 2019; Accepted 16 April 2019
Available online 06 May 2019

way catalyst to control exhaust pollutant emissions [5].

One of the most attractive solutions to improve the efficiency in SI engines is the lean burn concept, which consists of operating the engine in lean conditions ($\lambda > 1$) [6]. This increases the engine efficiency due to the reduction of the heat losses through the combustion chamber walls, the increment of the specific heats ratio (γ) and the reduction of pumping losses at part-loads [7]. However, the state-of-the-art three-way catalysts are not compatible with the lean burn concept [8] and then the nitrogen oxides (NO_x) emissions limit imposed by the standards can only be reached by increasing the dilution ratio up to λ levels over 1.8–2.0 for gasoline-like fuels [9]. However, this solution deals to critical ignition and flame propagation issues [10], so these extreme lean mixtures promote the cycle-to-cycle variability and increase the probability of flame quenching or even misfire, with the associated increment in related emissions [11].

Another commonly applied strategy to improve the SI engine efficiency consists in keeping the stoichiometric air-to-fuel ratio ($\lambda = 1$) and diluting the oxygen concentration in the mixture by introducing Exhaust Gases Recirculation (EGR) [12]. This option has the evident advantage of being fully compatible with the three-way catalyst for pollutant control, particularly NO_x emissions [13]. However, the EGR rate necessary to decrease NO_x down to the emissions standards without the aftertreatment system is around 50%, which leads to the same issues as increasing the air-to-fuel ratio in terms of cycle-to-cycle variability, flame propagation and misfire [14].

The pre-chamber ignition concept, also known as Turbulent Jet Ignition (TJI) [15,16], arises as a very promising alternative for enabling the implementation of the previous strategies overcoming their drawbacks in SI engines from high power stationary powerplants [17] to automotive applications [18]. This ignition concept uses a conventional electrical spark system to ignite a given amount of fuel/air mixture in a dedicated volume (pre-chamber) connected to the combustion chamber (main chamber) through a set of orifices [19]. Combustion increases the pressure in the pre-chamber so a set of jets are ejected towards the main chamber, forcing the onset of combustion in multiple locations and also sweeping the main chamber volume [20]. The details of the complex characteristics of the ejected jets have been thoroughly discussed in the literature [21,22]. The kinematics and development of the emitted hot jets from the pre-chamber were studied by Allison et al. [23], while other authors analysed different multi-jet configurations to understand their interaction and its influence of the flame shape inside the main chamber [24]. In suitable conditions, the main chamber combustion shows extremely low dispersion and it is significantly faster compared to the conventional spark-ignition system [25]. In general, this faster combustion is also favourable to mitigate the knock tendency, allowing an increasing compression ratio to further improve the engine thermal efficiency [26].

The pre-chamber ignition concept can be implemented according to two approaches [15,16]. In active systems [27], there is a dedicated fuel supplier inside the pre-chamber, thereby its air-to-fuel ratio is controlled at optimum values around 1, independently from that of the main chamber. In this region, the desired lambda value, usually gathered between 2.0 and 2.4 for gasoline fuel, is fixed by the main injector. In lean burn conditions, with air-to-fuel ratios well over 1 in the main chamber, the high reactivity of the ejected jets from the pre-chamber promotes the ignition of the main chamber charge. Other benefits associated to this active system are the stratification of the charge and the sharp reduction of the emitted HC and NO_x [28]. In passive systems [29], there is no additional fuel addition in the pre-chamber, so its air-to-fuel ratio is not directly controlled. In port fuel injection (PFI), engines λ is essentially equal in both chambers, while in direct injection (GDI) engines λ differences between chambers can be indirectly generated by adjusting the pre-chamber and injector relative spatial position up to a some extent [30].

In short, the key advantage of passive systems is its mechanical simplicity as the pre-chamber can be directly assembled into a conventional spark plug body, making the implementation straightforward in terms of packaging and costs. However, some aspects should be still investigated in detail, for example, the pre-chamber scavenging and filling, which depends basically on the gas transfer between the pre-chamber and the main chamber, and the limits of the concept in terms of maximum air and/or EGR dilution.

The pre-chamber ignition concept has been widely investigated due to its unquestionable advantages and performance [31]. Particularly, the increased combustion velocity [32,33], the reduced cycle-to-cycle variability [31] and its capacity to operate under lean burning conditions [34], make the active pre-chamber concept an interesting technology to improve the fuel economy in the transportation sector [35]. However, the extra cost of the double injection system compromises its application to automotive applications, especially in passenger cars, in which the packaging and manufacturing costs are critical and they could determine the success or failure of the concept itself. For this reason, the passive concept arises as a promising solution to overcome these limitations while decreasing the fuel consumption in the new generation of SI engines [31].

The research work reported in the present paper frames in the context of increasing the thermal efficiency and reducing the pollutant emissions of the next generation of SI engines, which is currently of great interest for the scientific community and of great concern for the society and worldwide governments. The potential of the passive pre-chamber ignition system is widely investigated following two stages. In the first stage, a 1D Wave Action Model (1D-WAM) of the experimental facility was built to analyse the impact of the most relevant geometrical parameters on the performance of the concept, defining two pre-chamber designs. In the second stage, these two designs were experimentally evaluated by comparing the results against those obtained with a conventional spark-ignition concept to identify their benefits/drawbacks, and also to discuss the suitability of the passive pre-chamber ignition concept to extend the λ or the EGR rate limits.

2. Tools and methodology

2.1. Engine architecture and test cell characteristics

Experimental activities were carried out in a single-cylinder research version of a 4-Stroke turbocharged SI engine well representative of those currently employed in passenger car applications. As a reference, Table 1 contains the most relevant characteristics. The engine compression ratio was increased up to 13.6 with the aim of checking the compatibility of the lean burn or EGR dilution combined with the passive pre-chamber ignition concepts with high compression ratios. The original GDI fuel supply system was replaced by a PFI system assembled in the intake manifold at 270 mm from the cylinder head in order to generate a fully homogeneous air/fuel mixture inside the cylinder, avoiding possible uncertainties generated by uncontrolled heterogeneities. Cylinder head has four valves with double-overhead camshafts allowing to improve the cylinder scavenging and filling, since the valve overlap was intentionally removed with the aim of avoiding shortcircuit losses.

As shown in Fig. 1, the conventional spark plug and the spark plug

Table 1
Main specifications of the engine architecture.

Engine	4-stroke SI
Number of cylinders [–]	1
Displacement [cm^3]	404
Bore – Stroke [mm]	80.0–80.5
Compression ratio (geometric) [–]	13.4:1
Valvetrain [–]	DOHC
Number of valves/cylinder [–]	2 intake and 2 exhaust
Fuel injection system [–]	PFI (P_{max} 6 bar)

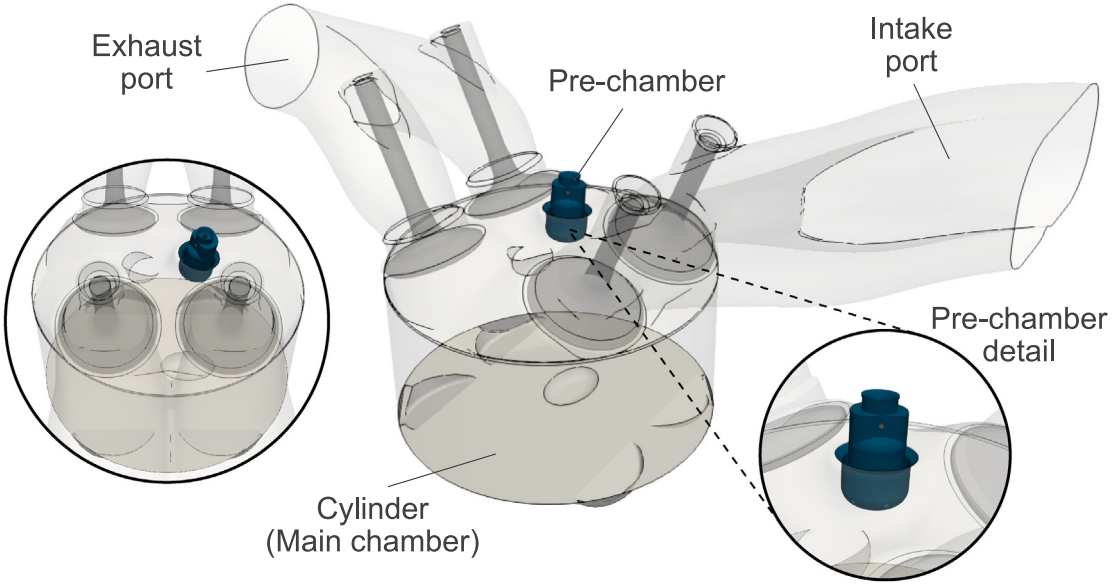

Fig. 1. Sketch of the engine design including the passive pre-chamber spatial positioning in the cylinder head.

body with an integrated pre-chamber share the same housing in the cylinder head, being easy and quick to exchange between concepts and/or pre-chambers.

The engine was assembled into a fully instrumented test cell according to the scheme shown in Fig. 2. Compressed air was provided by an external compressor to simulate boost conditions, while the exhaust backpressure was reproduced and controlled by means of a throttle valve placed in the exhaust line after the exhaust settling chamber. The experimental facility also included a low pressure EGR system, designed to provide arbitrary levels of cooled EGR even at very high intake boost pressures.

Water and oil cooling circuits are also independent from the engine, and temperatures were strictly controlled and monitored during all experimental tests by an AVL 577 conditioner. The fuel consumption of the engine was monitored with an AVL 733 gravimetric dynamic fuel meter, and fuel temperature was controlled by an AVL 753 conditioner. Tests were carried out using a calibrated gasoline with the 95 Research Octane Number (RON95) fuel shown in Table 2.

Pollutant emissions from the engine were sampled close to the exhaust settling chamber and routed to a gas analyser HORIBA MEXA 7100 DEGR by a heated pipe to ensure gas temperatures above 150°C. Measurements of O_2, CO, CO_2, HC, NO_x and EGR rate were performed

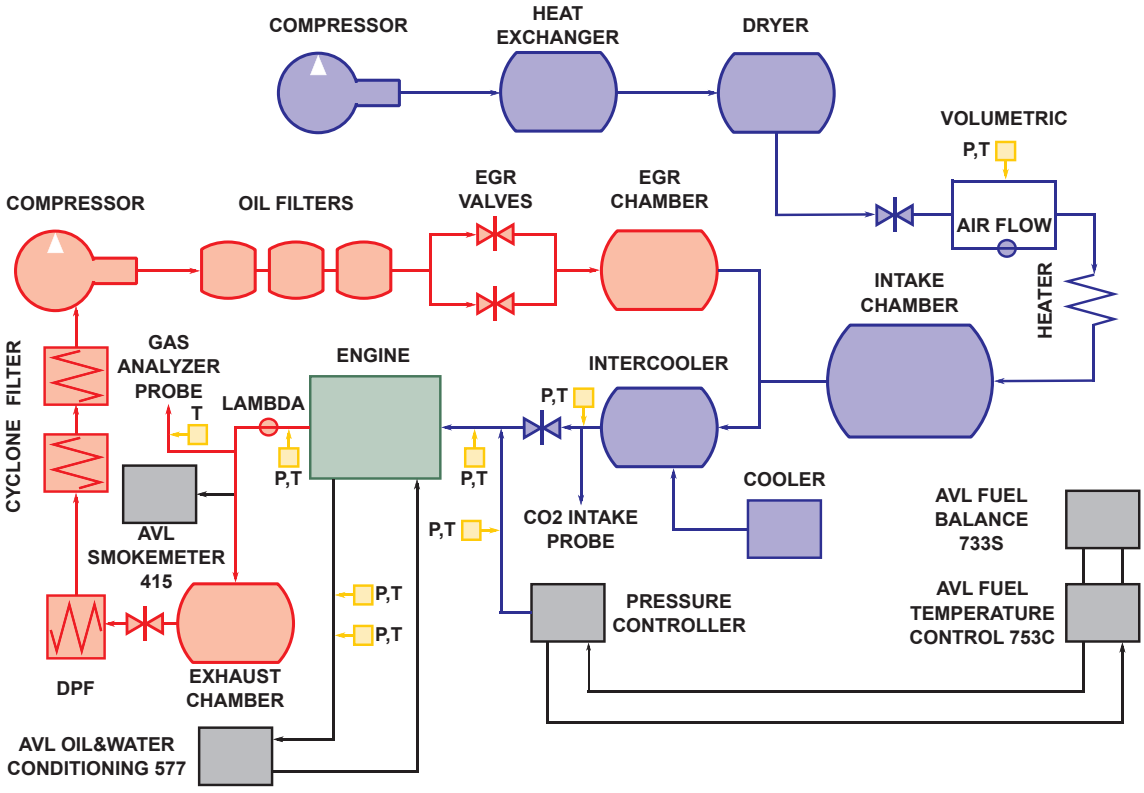

Fig. 2. Complete layout of the engine test cell.

Table 2
Main chemical and physical properties of the used fuel.

Type	Gasoline RON95
H/C ratio [mol/mol]	1.761 mol/mol
O/C ratio [mol/mol]	0.0 mol/mol
Oxygen content [%]	0.0
A/F_{st} [–]	14.374
Lower Heating Value (LHV) [MJ/kg]	42.793
Density (15ºC) [kg/m^3]	843.8
Kinematic viscosity (40ºC) [cSt]	2.47
Reduced formula ($C_xH_yO_z$)	7.594 (x) − 13.376 (y) − 0.0 (z)

for all tests, while soot emissions traced by the filter smoke number (FSN) were measured by an AVL 415 Smokemeter. Finally, the average air-to-fuel ratio was calculated dividing the fresh air mass flow rate, excluding the air present in the EGR, by the injected fuel mass flow rate. In-cylinder air-to-fuel ratio was measured by the gas analyzer HORIBA MEXA 7100 DEGR and also by a lambda sensor at the exhaust. Instantaneous cylinder pressure was measured using a piezoelectric sensor, while instantaneous intake and exhaust pressures were measured using piezorresistive sensors. All high frequency signals were sampled with a resolution of 0.2 cad.

The most relevant global parameters related to the combustion process, such as the indicated gross mean effective pressure (IMEP), start of combustion (SoC), combustion phasing (CA10 and CA50), combustion duration (CA1090), maximum cylinder pressure, pressure gradient, combustion stability, heat release rate (HRR) and cylinder mean gas temperature were calculated from the cylinder pressure signal by the in-house 0D combustion diagnostics software [36,37].

2.2. 1D Wave Action Model

A complete 1D Wave Action Model layout of the experimental facility and the single cylinder engine was generated after gathering the required geometric information of the different elements. The model was constructed in two stages: initially, a basic layout of the engine and test bench—including air, EGR and fuel supplies—was defined, and later, the dedicated layout of the pre-chamber was developed and connected to the engine cylinder volume by a set of ducts representing the pre-chamber orifices.

Regarding the combustion process simulation, two different approaches were followed according to the experimental information. The HRR profile was imposed in the main chamber coming directly or indirectly, after a proper scaling, from thermodynamic analysis of the experimental instantaneous cylinder pressure. Since the instantaneous pressure within the pre-chamber was not available, HRR profiles were case-generated using a Wiebe function [38] with the proper shape parameters required to match the desired combustion shape and duration.

For validation purposes, the reference model layout—without the pre-chamber—was calibrated by comparing its results with those obtained after testing the engine with the conventional spark-ignition system. In particular, tests were performed at the target operating condition described in Table 3. Results shown in Fig. 3 shown that intake and exhaust acoustics are fairly reproduced by the model whereas the prediction error of the air/fuel mass flow rate is lower than 2%. As it can be seen in Fig. 4, the pressure profile during the closed-cycle is also accurately reproduced by the model. In addition, the peak pressure error is lower than 3% leading to a similar error in the gross IMEP estimation.

In sum, results confirm how the developed 1D-WAM model is suitable for the further research activities since its capability to reproduce the experimental trends have become evident.

Table 3
Details about experimental baseline test conditions.

Spark-Ignition baseline	
Engine speed [rpm]	4500
IMEP [bar]	12.5
Injected fuel [mg/cp]	28.6
Intake air temperature [K]	283
Intake pressure [bar]	1.1
Exhaust pressure [bar]	1.07
Coolant and oil temperature [K]	363

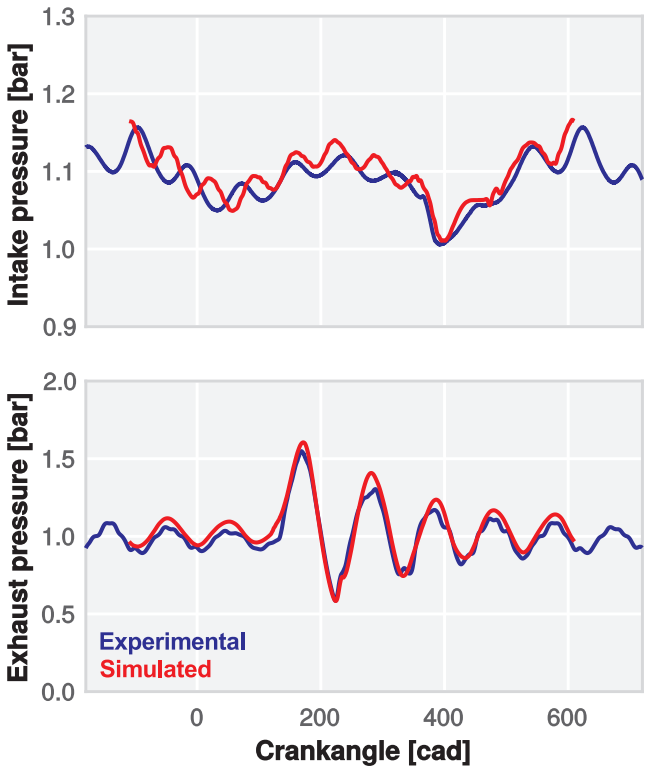

Fig. 3. Comparison of experimental and simulated (1D-WAM model) intake and exhaust pressures.

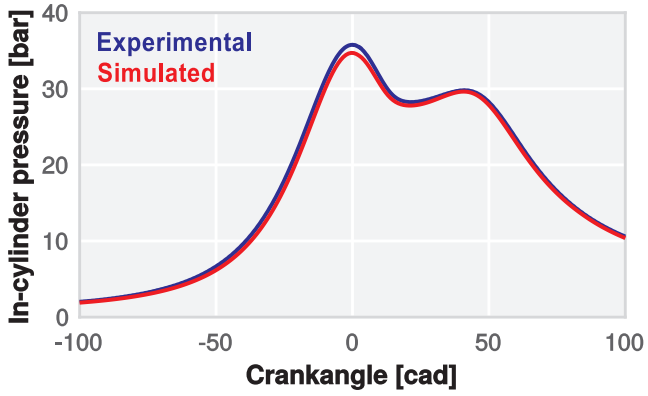

Fig. 4. Comparison of experimental and simulated (1D-WAM model) in-cylinder pressure profiles.

2.3. Methodology

In this research, the target operating condition was selected by considering different aspects. The combination of medium-to-high engine speed (4500 rpm) and mid-to-high engine load (12.5 bar IMEP) has

not been extensively investigated previously, so there is not much information reported in the literature. The mid-to-high engine speeds compromise the scavenging and filling of the pre-chamber, which is critical in passive systems as discussed in the introduction, so assuring the proper gas exchange at this point is critical for the applicability of the passive pre-chamber ignition concept. The mid-to-high engine load was selected to investigate the impact of the passive pre-chamber ignition concept on knocking tendency. However, staying in the safety side was mandatory in both cases, so higher speeds/loads were considered risky for the engine structural integrity, particularly considering its high compression ratio. After the definition of the target operating condition, this research work has been divided into two chronological stages following a logical structure.

As a first stage, a 1D-WAM simulation—including the pre-chamber sub-model—was performed with the aim of performing a qualitative analysis of the impact of the most relevant passive pre-chamber geometrical parameters on its performance, as other authors did in prior works [39,40]. Then, two pre-chamber designs were manufactured and experimentally tested. The parameters under consideration were the pre-chamber volume and the diameter of the orifices, always keeping the number of orifices (6). Regarding the pre-chamber volume, it was controlled by adjusting its length since the diameter was constrained by the cylinder head housing.

Several assumptions were required as these pre-chambers were not available at this point for the experiments, consequently experimental data was not accessible for validation. Thus, the main-chamber combustion was modelled by imposing the HRR profile obtained after scaling the experimental trace of the reference case operating with the conventional spark-ignition system.

According to the literature [25], the pre-chamber ignition concept shortens the combustion duration between 2.0 and 3.0 times, therefore the scaling factor was adjusted so that the combustion duration was 2.5 times shorter [27]. The phasing was kept constant at 50% of fuel burned (CA50) and equal to 24.2 cad, which corresponds to Maximum Brake Torque (MBT) conditions. Pre-chamber combustion was modelled by a Wiebe function [38] with the proper parameters to generate a 29 cad combustion duration for a pre-chamber volume of 600 mm^3. This duration was linearly scaled with the pre-chamber volume. Since the pre-chamber geometry is a cylinder, the length to be travelled by the front flame—assuming constant turbulent flame speed—practically coincides with the length of the pre-chamber. The CA50 of this combustion was fixed to coincide with the onset of the main-chamber combustion. Lastly, the total injected fuel was kept constant at the reference value (3.85 kg/h), therefore, the study was performed at iso-total fuel energy conditions.

With all these assumptions a test grid, witch combines pre-chamber volumes between 400 and 1000 mm^3 (7 levels) and orifice diameters among 0.4 and 0.9 mm (6 levels), was defined, resulting in 42 simulations all performed under stoichiometric conditions. The analysis of the performance of the pre-chambers was focused on the total fuel quantity available at the start of the pre-chamber combustion and the maximum Δp achieved between both chambers during ejection event.

Finally, two pre-chamber designs were selected from this study for being experimentally evaluated. The first is considered as the most promising alternative, while the second one was chosen to be evidently worse.

As a second stage, an experimental campaigning was carried out in the engine in order to compare the performance of the two passive pre-chamber geometries against the conventional spark-ignition system. All tests were designed for being fully compatible with the previous modelling activity, so in each case the spark timing was swept until reaching the MBT conditions. In addition, the injected fuel mass was calibrated to obtain the target gross IMEP operating with the conventional spark system at stoichiometric conditions without EGR and then, it was kept constant for all other tests. Initially, the conventional spark system and the two passive pre-chamber designs were evaluated at these conditions to gain knowledge on the benefits/drawbacks of this ignition concept.

Later, all three ignition systems were evaluated in lean burn conditions by increasing the air-to-fuel ratio in steps of 0.2 until reaching the maximum acceptable level (limited by combustion stability). The study was completed by assessing the systems in diluted conditions by increasing the EGR rate in steps of 10% also until finding the maximum value from which the combustion stability was unacceptable. Details of the tested cases are included in Table 4. Experimental results were expected to support or reject the modelling analysis and design process followed in the previous stage.

Table 4
Operating settings for tests at 4500 rpm 12.5 bar IMEP.

	λ [–]	EGR [%]
Spark-ignition	1.0–1.2–1.4	0%–10%–20%
Pre-chamber 1	1.0–1.2–1.4–1.6	0%–10%–20%
Pre-chamber 2	1.0–1.2	0%

3. Results and discussion

This section describes the main findings of the present investigation starting from the design of two passive pre-chamber geometries, which are lately experimentally evaluated operating in stoichiometric conditions, and completing the study by assessing their performance in combination with the lean burn and EGR diluted combustion concepts.

3.1. Design of the passive pre-chamber geometry

Results of the aforementioned methodology for designing the pre-chamber geometry are presented in Fig. 5. In this figure, all the relevant parameters were plotted using a cubic polynomial fit for visualization. Also, the region where there is no ejection process was not coloured. As can be seen, this method allows to identify optimum design parameters (pre-chamber volume and holes diameter) taking into account multiple aspects.

The maximum Δp achieved is directly related to the capability of the jets to penetrate into the main combustion chamber. This parameter is calculated as the pressure difference between the main chamber and the pre-chamber. The higher Δp, the less time the jets need to sweep the main chamber. The amount of fuel available within the pre-chamber at the spark plug ignition, denoted *fuel@SoC*, indicates the maximum amount of energy that is possible to obtain from the pre-chamber combustion. Lastly, the *total burned fuel* parameter is the fraction of this fuel that is really consumed. The difference between both parameters is related to the fuel mass evolution inside the pre-chamber during the combustion process. As the flame front progresses, pressure inside the pre-chamber rises and forces the air-fuel mixture to leak through the orifices. On the contrary, for cases with low Δp, the pressure difference between the pre-chamber and the main chamber inverts before the end of the pre-chamber combustion, and additional fuel is injected into the pre-chamber, thereby leading to an increased *total burned fuel* value that exceeds the fuel mass available at SoC (*fuel@SoC)*.

According to these parameters, it can be observed that there are two different regions in the simulated space. While the top-left region show the best combination of parameters, the region located at the bottom-right side of the graphs congregate the worst designs.

Due to the novelty of this ignition system and the lack of available information about it, two different designs were chosen. The first one, named pre-chamber 1, is located in the favourable region where the achieved Δp assures a suitable jet features. The second design, referred as pre-chamber 2, is localized in the unfavourable region, thereby a considerable lack of performance was expected from it. The weak performance of the second pre-chamber can be explained by the small jets penetration and the low fuel available for the pre-chamber

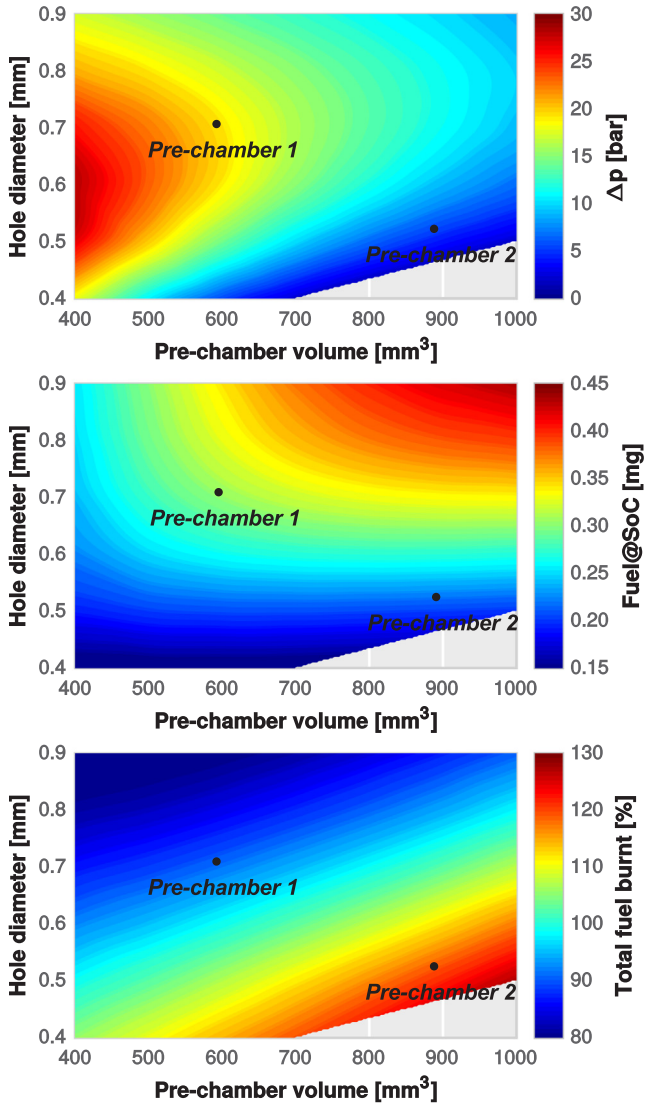

Fig. 5. Results of the parametric study performed with the 1D-WAM code for designing the pre-chamber.

combustion.

Considering these extreme configurations will help to further validate the pre-design method presented here, thus assuring a good estimation of the combustion system in the whole considered range of application. The validation of this method is particularly critical in order to verify if this simple and computationally inexpensive method could shed some light in the design of this complex ignition system.

The specific geometric parameters of both selected pre-chambers are shown in Table 5. As it can be seen, the favourable design has smaller volume and higher orifices diameter.

Recalling the maximum Δp graph already shown in Fig. 5, it can be seen that the pre-chamber 1 has larger values than pre-chamber 2. As the corresponding contour plot shows, this value is considerably higher in the pre-chamber 1 than in pre-chamber 2 reaching almost 15 bar of

Table 5
Main geometric specifications of the designed pre-chambers.

	Pre-chamber 1	Pre-chamber 2
Volume [mm^3]	600	900
Hole diameter [mm]	0.7	0.5
Number of holes [–]	6	6

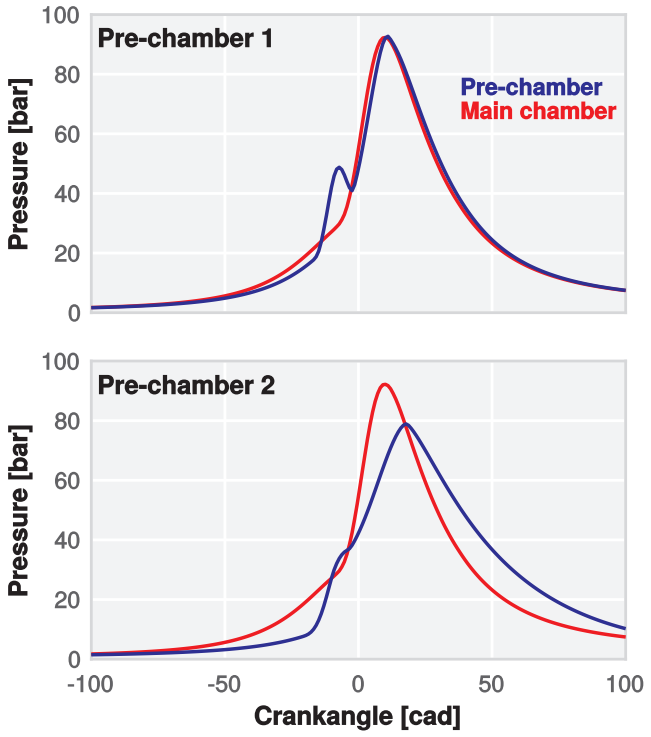

Fig. 6. Simulated pressure profiles for the main chamber and pre-chamber for the selected designs.

difference. Consequently, jets ejected from pre-chamber 2 will have more difficulties to penetrate within the main combustion chamber, compromising not only the turbulence intensity—which helps to enhance the burning velocity—but also reducing the reaction surface in contact with the unburned charge.

It may be easy to think that larger pre-chamber volume increases the Δp and then the performance of the jets, since the amount of fuel in the pre-chamber should be higher. Moreover, mass flow losses from the pre-chamber increase as the holes diameter is enlarged, causing that the optimum solution will be a balance between the volume and cross-sectional area of the orifices. In this way, pre-chamber 1 design has an adequate ratio between both parameters whereas pre-chamber 2 has a combination of a big volume and small orifices.

Fig. 6 shows a comparison among both selected designs. In this figure, the pressure evolution in the main chamber and in the pre-chamber is plotted to identify the differences between both regions, and both designs as well. Moreover, it provides a better understanding of the pre-chamber filling process.

Examination of the top graph allows to distinguish three different stages during the closed-cycle. First, the pre-chamber is filled with the unburned charge available in the main chamber. The pressure in the main chamber is higher than in the pre-chamber during this stage as a consequence of the pressure drop though the pre-chamber orifices. This effect is more noticeable in the second pre-chamber design, in which the pressure drop is significantly higher due to the smaller orifices diameter. The second stage corresponds to the pressure rise due to the pre-chamber combustion. The charge is burned after the spark onset, increasing the pressure inside the pre-chamber. Then, a mixture of unburned charge and combustion products, including intermediate species at high temperature, flows into the main chamber in the form of jets. In the final stage, these high-reactivity jets ignite the charge in the main combustion chamber, releasing most of the energy.

3.2. Experimental evaluation of the pre-chamber designs

After the design process, the selected pre-chambers were fabricated

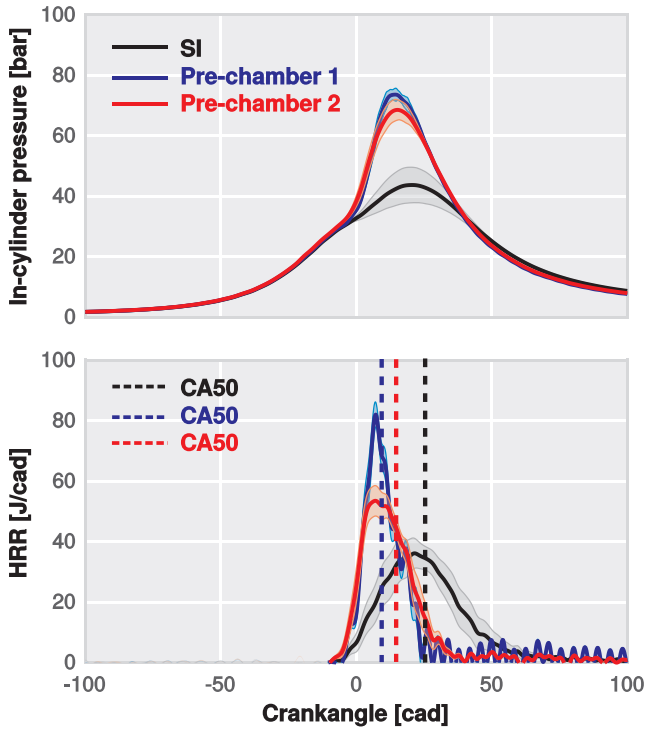

Fig. 7. Effect of pre-chamber 1 and 2 on combustion. In-cylinder pressure and HHR profiles for SI, pre-chamber 1 and pre-chamber 2 at stoichiometric conditions.

and assembled in the engine in order to test them and validate the design methodology. Three ignition systems were tested (SI, TJI pre-chamber 1 and TJI pre-chamber 2) at conditions described in Table 3 without EGR dilution and $\lambda = 1$ conditions.

The measured in-cylinder pressure and the estimated HRR profiles of these tests are included in Fig. 7. The cycle-averaged cycle is plotted together with the standard deviation data to analyse the cycle-to-cycle variation (CCV). It can be clearly seen how there is a substantial increment of the maximum pressure (nearly 50%) when switching from SI to TJI concept. This increment is mostly produced by the higher burning rate reached by the pre-chamber ignition concept that optimizes the combustion phasing, as the bottom graph of the figure shows. The combustion duration is remarkably reduced—from 39.6 cad to 20.8 cad—by the TJI concept whereas the combustion phasing (CA50) is moved towards the Top Dead Centre (TDC).

It is also noticed from Fig. 7 that the standard deviation decreases almost 80% when operating with TJI concept. This reduction is more evident in Fig. 8 in which the σIMEP is plotted for the three ignition concepts considered so far. In addition, the increment in IMEP combined with this CCV reduction leads to an increment of the gross indicated efficiency of 3%.

Regarding pollutants, it is observed that hydrocarbons (HC) and carbon monoxide (CO) emission are kept constant at stoichiometric conditions, maintaining the combustion efficiency at similar values as those shown by the SI concept. This trend is also accompanied by an increase of NO_x emissions caused by the higher local temperatures achieved when operating with TJI.

Therefore, the overall performance of the engine at this particular operating condition can be improved by switching to the passive TJI injection system. The values obtained by both pre-chambers are very similar in terms of performance.

3.3. Towards lean combustion conditions

Once that both pre-chambers designs have been tested at

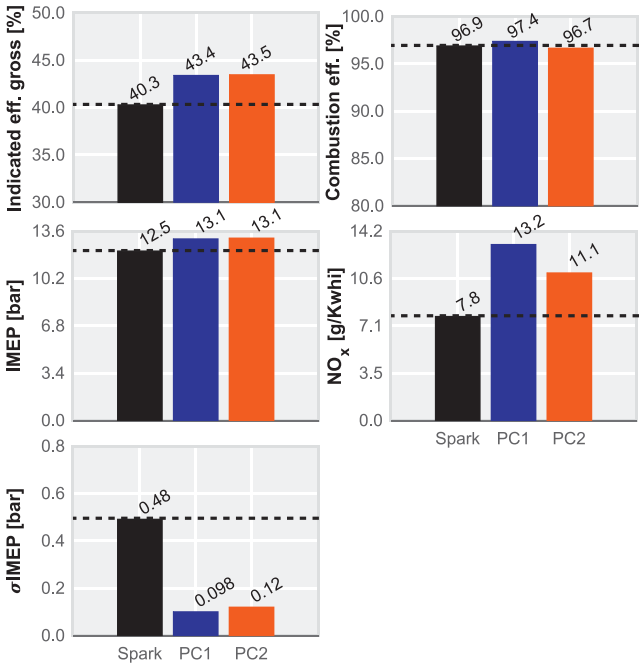

Fig. 8. Gross indicated and combustion efficiency, IMEP, σIMEP, and NO_x at stoichiometric conditions tests for spark-ignition (Spark), TJI pre-chamber 1 (PC1) and TJI pre-chamber 2 (PC2).

stoichiometric conditions, the next step in the investigation was to evaluate the performance of the TJI concept under lean combustion conditions. In particular, the target of this study was to extend the operating range to $\lambda = 2$ conditions at which the exhibited NO_x levels are well bellow the stipulated limits without the use of the three-way catalyst.

The effect of increasing the air-to-fuel ratio is shown in Fig. 9. For this study, λ was swept from 1 to the ignition limit of each combustion concept considered. In all these tests, the combustion phasing was fixed by the maximum brake torque (MBT), or by the knock limit (if the latter

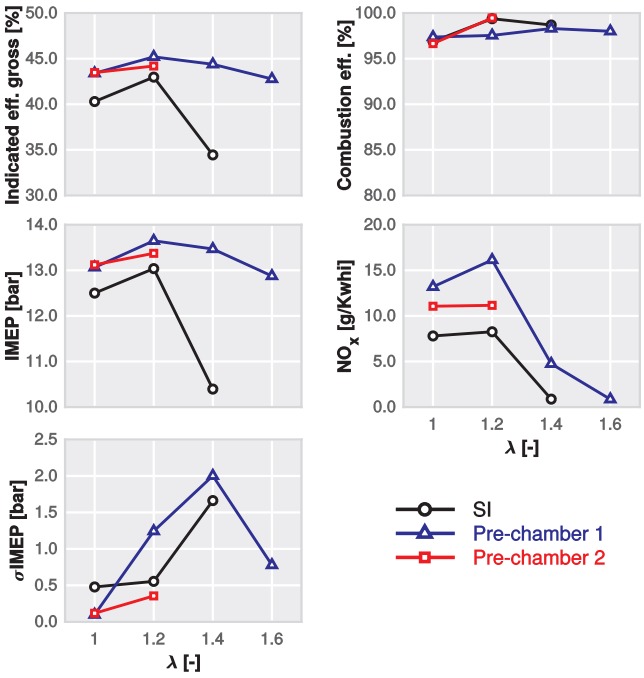

Fig. 9. Effect of increasing the air-to-fuel ratio over the main operating parameters and emissions levels.

could not be met) to assure the maximum output power.

As seen for the stoichiometric tests, TJI offers higher levels of efficiency. Both pre-chamber designs show higher IMEP values than the conventional SI concept in their respective operating λ ranges. In addition, the combustion stability is maintained at comparable and reasonable levels ($\eta_c > 97.5\%$) under all tested conditions. However, the reduction in σIMEP already observed in the stoichiometric tests is not observed in the whole range of λ. Particularly, combustion of pre-chamber 1 becomes more unstable at $\lambda = 1.2$ and $\lambda = 1.4$ and the levels of σIMEP exceed those observed in the SI concept.

The higher temperatures achieved due to the TJI enhanced combustion lead to an increase in NO_x emissions whereas trends are quite similar in both concepts. In addition, TJI with pre-chamber 1 ($\lambda = 1.6$) is able to reach same NO_x levels as SI ($\lambda = 1.4$) without the considerable loss of efficiency. Nonetheless, despite being significantly reduced, NO_x levels are still far from the target limits imposed by public institutions for the near future.

It can be observed in Fig. 9, that λ sensitivity not only depends on the combustion concept, but also the pre-camber design plays a relevant role in the ignition limit. Other important aspect to highlight is that SI concept is capable to extend the ignition limit with an evident IMEP drop whereas both TJI concepts keep the IMEP at competitive values until the engine shuts down. In order to understand these trends, Fig. 11 show the in-cylinder pressure and HRR of the three concepts at their respective ignition limits. The most significant difference arise in the morphology of the combustion law. While the length of the SI combustion is considerably enlarged when the air dilution is increased, it hardly changes when operating with both TJI concepts. Consequently, the combustion phasing (CA50) can be delayed far beyond the TDC in the SI concept.

What is evident from these results is that the ignition issues observed in the main chamber when operating with conventional SI are replicated in the pre-chamber at different scales, depending on the thermochemical and turbulence conditions. Hence, the decreased fuel mass inside the pre-chamber as the air-to-fuel ratio is increased, clearly compromises the ignition and the subsequent mixture burning. However, the increased ignition limit shown by the pre-chamber 1 can be explained probably due to the enhanced turbulence conditions inside the pre-chamber that promote a faster combustion, resulting in enhanced jet features to ignite the main chamber.

This situation worsens if it is considered that there is a certain amount of residual gases from the previous cycle that is not evacuated from pre-chamber during the scavenge. This extra dilution decreases the mixture reactivity and compromises the ignition. This effect becomes more evident in the pre-chamber 2, where the small orifices reduce the permeability between the pre-chamber and the main chamber, thereby reducing the combustion products exchange. Although the expected performance of pre-chamber 2 was worse than that obtained at $\lambda = 1$ conditions, it is clear that its operating range is more limited and the tolerance to air dilution is considerably lower than pre-chamber 1. This fact validates the design methodology described in Section 2 since the overall results observed from pre-chamber 2 are generally worse than those obtained from pre-chamber 1.

Although the experiments show a fair coherence with the 1D-WAM model results, the numerical solution should be directly contrasted with experiments to determine whether the design methodology is valid and sufficiently robust. In this way, Fig. 10 shows the result of this comparison considering the baseline operating condition (4500 rpm and 12.5 bar IMEP) for the pre-chamber design 1. As can be seen, results reveal a reasonable agreement between both experiments and simulation. Therefore, the capacity of the numerical model for predicting experimental trends with a low computational cost is demonstrated. These results also unveil the potential advantages of this numerical methodology when optimizing the pre-chamber design since a huge number of parameters can be tested without the need of costly and time-consuming experimental tests.

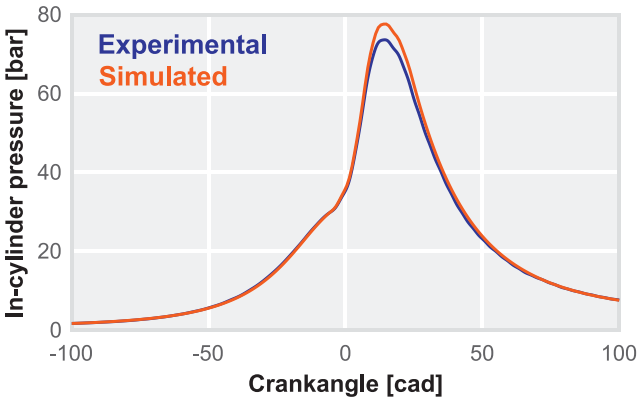

Fig. 10. Comparison of experimental and simulated (1D- WAM model) in-cylinder pressure profiles for pre-chamber 1.

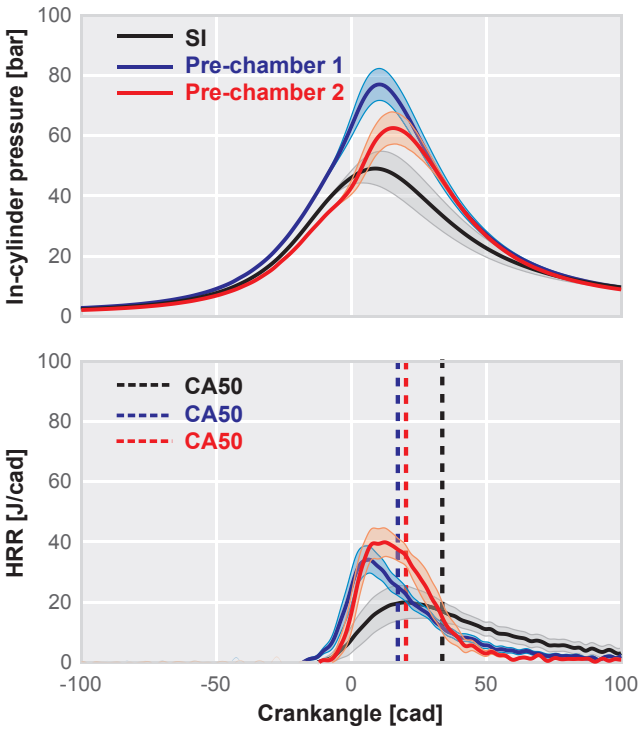

Fig. 11. In-cylinder pressure and HRR traces at the ignition limit for all considered combustion concepts. Black lines correspond to SI at $\lambda = 1.4$, blue lines refer to TJI pre-chamber 1 at $\lambda = 1.6$ and red lines to TJI pre-chamber 2 at $\lambda = 1.2$. (For interpretation of the references to color in this figure legend, the reader is referred to the web version of this article.)

Taking advantage of the 1D-WAM model results used for the pre-chamber design, it is also possible to estimate the amount of residual gases inside the pre-chamber at the start of combustion (SoC). Considering stoichiometric conditions and 0% of EGR dilution the predicted internal gas recirculation (IGR) rate is 14.7% and 26.1% for pre-chambers 1 and 2, respectively. These values explain the extremely reduced λ range showed by the pre-chamber 2, since the high IGR rates observed in the second pre-chamber results in a extremely diluted mixture out of the limits of inflammability.

From a theoretical point of view, efficiency can be expected to systematically increase with the air-to-fuel ratio due to the heat transfer reduction and increased specific heats ratio ($\gamma_{fuel} < \gamma_{air}$). However, recalling the evolution of the indicated efficiency of pre-chamber 1, it can be seen how it decreases after the maximum point achieved at $\lambda = 1.2$.

In order to find the explanation to this behaviour, a combination of

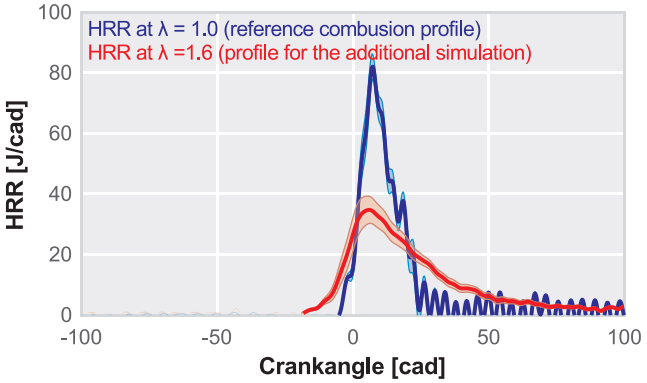

Fig. 12. HRR profiles used for the simulated λ swept performed in 1D-WAM. Both profiles correspond to the experiments at $\lambda = 1$ and $\lambda = 1.6$.

experimental results and the 1D-WAM modelling were used. In a first step, a complete λ sweep maintaining the combustion velocity equal to the $\lambda = 1$ test (experiment) was simulated, that is keeping the HRR profile in all simulations. This could help to understand how the efficiency evolves in the hypothetical case that the combustion does not change when modifying the air-to-fuel ratio. However, as Fig. 12 shows, the HRR profile changes as the λ value increases. Therefore, the HRR profile obtained from the $\lambda = 1.6$ test (experiment) was used in the same analysis to estimate how the efficiency decays due to the modified combustion law.

The trend of the simulated efficiency is shown in Fig. 13 whereas the additional simulation with the $\lambda = 1.6$ HRR profile is also included. It is observed from this figure that the indicated efficiency constantly grows as the air-to-fuel ratio is increased, when the combustion law is maintained. However, it drops four points when considering the real combustion law at $\lambda = 1.6$, reaching a value similar to that observed at $\lambda = 1$. This is also observed in the experiments (Fig. 9). Thus, as the combustion gets longer the maximum pressure, the combustion efficiency and stability decrease leading to a non-negligible loss of efficiency. In addition, simulation results have proved that the 1D-WAM model is a valuable tool not only for the pre-chambers design process but also to provide more insight about the experiments while contributing to the understanding of the complex phenomena linked to this particular ignition concept.

Fig. 14 includes the in-cylinder pressure and HRR traces for the $\lambda = 1.2$ tests, where the maximum efficiency is achieved for each combustion concept considered so far. As expected from the trends plotted in Fig. 9, the maximum in-cylinder pressure increases when switching from SI to both TJI concepts. This is a direct consequence of the higher burning rates achieved by both TJI concepts, as it can be seen in the bottom plot of Fig. 14. In all these tests, the spark timing

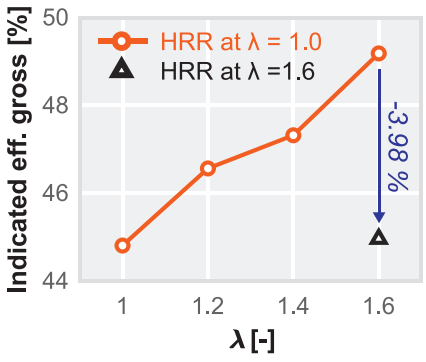

Fig. 13. Results of the gross indicated efficiency obtained from 1D-WAM simulations and experiments. The worsening of the predicted indicated efficiency is similar to the experiments.

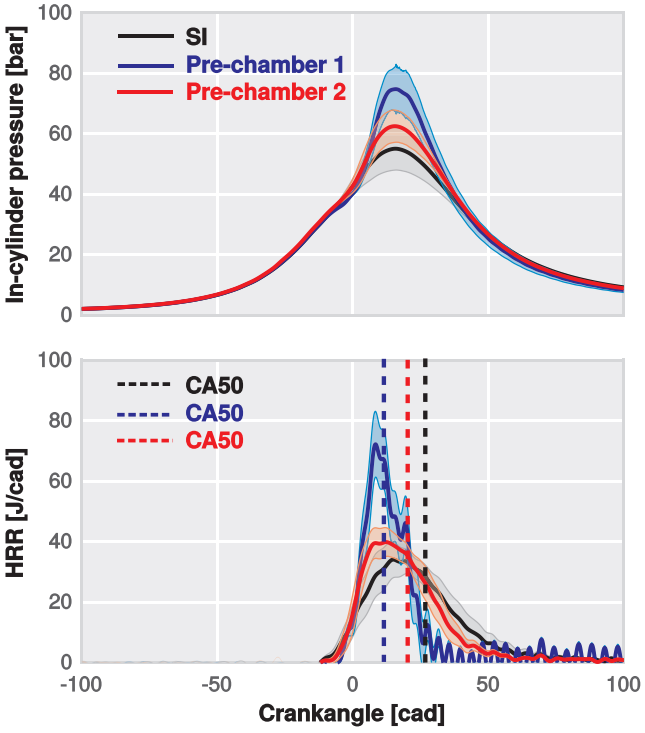

Fig. 14. In-cylinder pressure and HRR traces at $\lambda = 1.2$ conditions for all considered combustion concepts.

(ST), and then the start of combustion, was set when the maximum average knock intensity (MAPO) exceeds 1 bar (knock limit established by Kalghatgi et al. [41] and widely used in the literature).

In addition, there are two important things to highlight in this figure. The most evident is probably that the start of combustion is almost coincident in all cases while the duration of combustion changes in the different concepts. Thus, increasing the burning velocity and reducing the combustion duration, helps to phase the combustion process closer to TDC where the cycle efficiency is maximized. This fact evinces the suitability of the TJI concept to increase the engine efficiency when knock is the main constraint due to either, the low knock-resistance of the fuel (gasoline-like fuels with low RON numbers) or the design of the engine itself (high compression ratio, increased intake boosting, etc.).

However, in those combustion systems in which knock is not the major limitation, it is not clear which is the key aspect in the search for higher efficiency. Therefore, determining the influence of the combustion phasing and/or the combustion duration on efficiency can mean a step forward in understanding the concept operation while identifying its main drawbacks.

In view of this new emerging question, a further analysis was performed again with the help of the results provided by the 1D-WAM model. In this case, simulations were run again with a reference HRR profile (that measured at $\lambda = 1$ conditions). This reference profile was artificially adjusted to sweep both the start and the duration of combustion. The simulations grid resulted in 45 cases: five levels for the combustion duration (from the reference duration to three times its duration) and nine levels for the start of combustion (from -10.4 to 10.4 cad).

Results in terms of indicated efficiency are shown in Fig. 15. Experiments are also included in the figure to compare simulations and measurements. Empty regions correspond to those conditions out of the studied range. As the contour plot shows, the main cause of the efficiency variation is related to the combustion phasing (CA50) rather than the combustion duration (CA10-90). While the efficiency can be reduced by 5% when delaying the combustion phasing by 10 cad

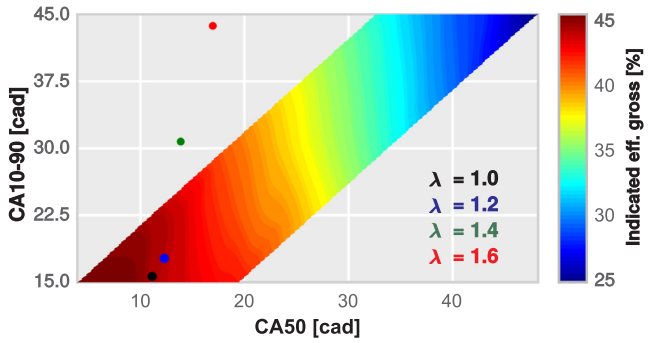

Fig. 15. Contours of gross indicated efficiency obtained from 1D-WAM simulations. The included points correspond to the experiments.

approximately, the combustion duration only has a negligible effect. Hence, these results explain why the TJI concept, although promoting a faster combustion process, is not able to keep rising the indicated efficiency as the air-to-fuel ratio is increased beyond 1.2. Moreover, they evince a new paradigm since it may be possible to optimize the combustion phasing and, therefore, the efficiency in those combustion systems where knock is the major constraint.

3.4. Towards EGR diluted combustion conditions

As in the prior section, in this second stage of the investigation the effect of the EGR dilution in the engine operation was analysed in detail. Experimental tests consisted in increasing the EGR rate until the combustion stability becomes unacceptable using both SI and TJI concepts. The spark timing was also fixed by the MBT and/or by the knock limit (MAPO > 1 bar).

In Fig. 16 trends of all relevant engine outputs are included. In this case, only results related to SI and pre-chamber 1 were considered due to the lack of performance observed when operating with pre-chamber 2. In particular, the tolerance of the this latter pre-chamber to EGR was below 5%. Therefore, pre-chamber 2 was discarded for this study due to the narrow operation range observed. In contrast with the previous

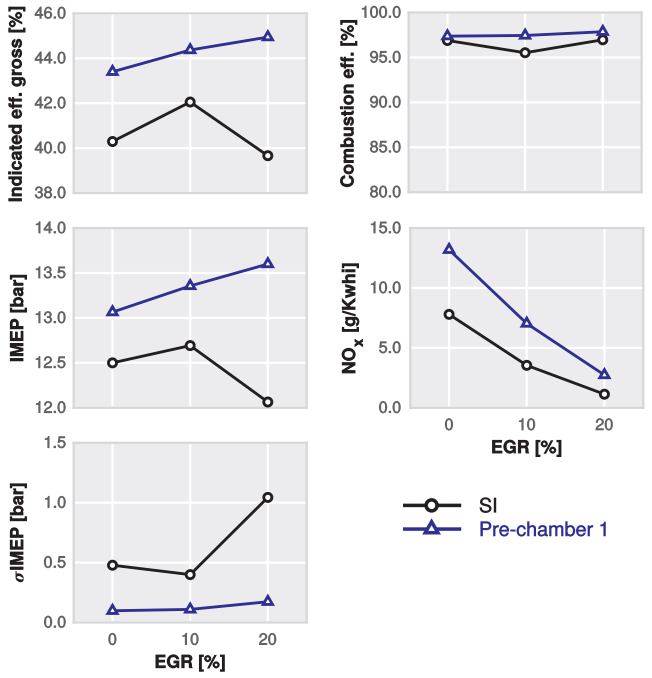

Fig. 16. Effect of increasing the EGR ratio over the main operating parameters and emissions levels.

study, the TJI concept has the same ignition limit than the conventional SI. It seems that the turbulence conditions in the pre-chamber do not contribute positively to the flame propagation progress and there is no appreciable gain when operating with the TJI concept. Thereby, the EGR limit is around 20% in both concepts.

One of the most interesting things to analyse there, is not only to check the tolerance of TJI concept to EGR dilution, but also to compare it with that observed when diluting the charge with air. It is quite evident that both concepts are more sensitive to dilution with EGR than with air, especially in the case of the TJI concept (pre-chamber 1) which shows a 40% less of tolerance.

Assuming that the turbulence intensity (u') and the integral length scale (l_t) do not vary when the dilution rate is increased, it is possible to obtain how combustion evolves in the flame regime diagram, also called Borghi-Peters Diagram [42,43]. This hypothesis is reasonable since neither the engine hardware nor the engine speed are altered.

Literature review on this regard [44,45] revealed that typical flames in conventional SI engines are characterized by moderate Reynolds numbers ($10 < Re < 100$) and Karlovitz numbers close or below 1. Therefore, these flame features belong to the named *corrugated flamelets* regime. According to the premixed flames theory [46] the entire reactive-diffusive flame structure (l_f) is embedded within eddies of Kolmogorov scale size, thereby the flame structure is modified by the turbulent field.

In Fig. 17, a Borghi-Peters diagram is presented, highlighting the region where conventional SI engines operate. Moreover, blue and black lines show how the flame features change as the dilution rate is increased. The reference turbulence parameters u' and l_f, were chosen arbitrary in order to focus the reference conditions (0% of dilution) inside the SI operation regime. The corresponding laminar flame features, laminar flame speed (s_L) and flame thickness (l_f), were calculated by the premixed laminar flame-speed model included in the commercial software CONVERGE [47]. Similar to an ideal case set-up to measure flame-speed, this code simulates the 1D flame in a channel with a fixed cross-sectional area at constant pressure. For this study, four air-diluted cases ranging from 0% to 80% and four additional ones ranged between 0% and 40% for EGR dilutions were calculated. This method allows to determine, at least in a qualitative way, which is the path travelled when modifying the dilution conditions.

Fig. 17 shows how increasing the dilution rate, either with air or with EGR, the flame features move towards the *thickened flame* regime, where the size of eddies becomes smaller than the flame thickness. In this way, some eddies penetrate into the diffusive flame structure, enlarging the front flame thickness whereas decreasing its laminar speed. This latter effect can be observed in Fig. 18, in which all computed laminar flame speeds and flame thickness are plotted against the dilution degree. Nevertheless, it can be also observed in the Borghi-Peters

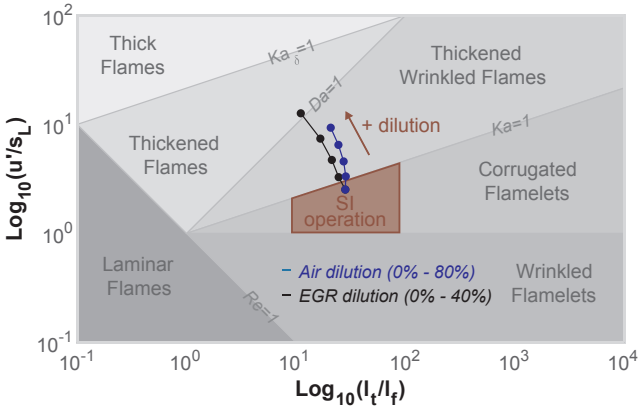

Fig. 17. Borghi-Peters diagram and trends observed when increasing the dilution rate with air and EGR.

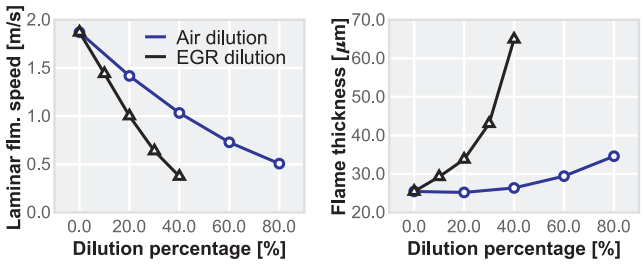

Fig. 18. Computed laminar flame speeds (s_L) and flame thickness (l_f) for air and EGR diluted cases.

diagram that the effect of EGR dilution is more marked since the flame reaches more unstable regimes (closer to $Ka_\delta = 1$ where the eddies can even penetrate into the reaction flame structure) with lower dilution rates. This behaviour can be explained by both the laminar flame speed reduction and the flame thickness enlargement observed in Fig. 18 when considering EGR to increase the engine efficiency.

Recalling to Fig. 16, though showing similar tolerance to EGR dilution, the TJI concept allows to increase the indicated efficiency until the ignition limit whereas the SI concept experiences a significant drop. The origin of these trends can be explained with the help of the conclusions obtained in the prior section and data displayed in Table 6.

Focusing on the SI concept, it can be observed how the increased efficiency when operating at 10% of EGR dilution is linked with an advanced combustion phasing (from 24.2 to 19.4 cad). Then, the efficiency drops below 40% when combustion is delayed up to 22.4 cad at 20% of EGR dilution. Regarding the TJI concept, the combustion phasing is advanced, or at least maintained, as the EGR dilution rises, thereby allowing to increase the indicated efficiency progressively with the EGR dilution degree. In all these cases (SI and TJI), the combustion duration stretches on as the EGR ratio increases, thus confirming the trends already seen in the previous section with the results of the 1D-WAM model.

Regarding the combustion stability, the TJI concept show improved values of σIMEP and combustion efficiency. NO_x emissions increase with respect to the SI concept. However, this is not so critical since the three-way catalyst is able to operate under these conditions.

Finally, the in-cylinder pressure and HRR traces of tests performed at 20% of EGR dilution are plotted in Fig. 19 to check how combustion is changing. Again, the maximum pressure for the TJI concept is higher than the spark-ignition concept. The peak of heat release rate becomes higher and combustion duration decreases.

4. Summary and conclusions

The present research has been focused on the implementation and evaluation of the Turbulent Jet Ignition concept for future turbocharged high-compression ratio spark-ignition engines. The final comparison between the results obtained with the Turbulent Jet Ignition concept against the conventional spark-ignition operation, provides an overview of the potential benefits and main drawbacks of this particular ignition concept when it is combined with lean burning and dilution

Table 6
Combustion phasing (CA50) and combustion duration (CA10-90) of all EGR tests.

EGR ratio	0%	10%	20%
	CA50 [cad]		
Spark-ignition	24.2	19.4	22.4
Pre-chamber 1	10.0	10.4	9.4
	CA10-90 [cad]		
Spark-ignition	39.6	42.0	58.2
Pre-chamber 1	20.8	25.2	36.0

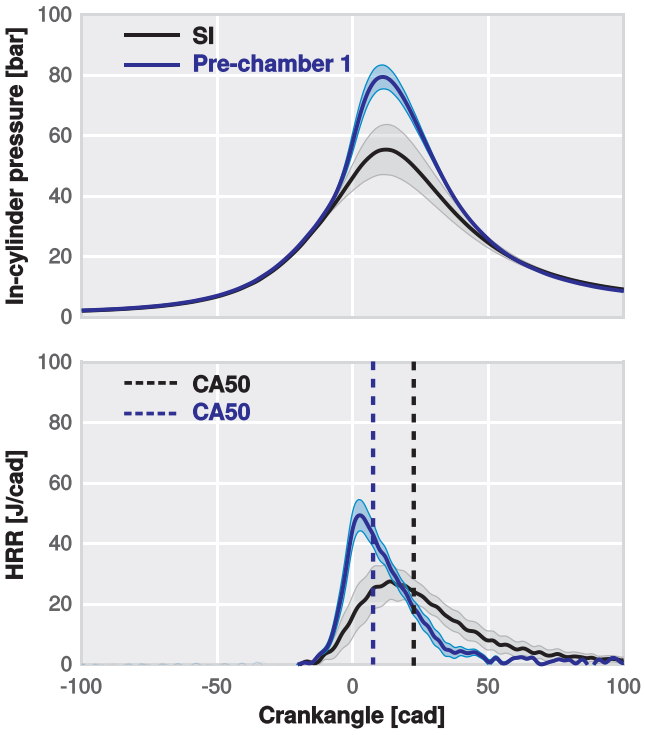

Fig. 19. In-cylinder pressure and HRR at 20% of EGR dilution.

with exhaust gases. Therefore, it represents a step forward in the understanding of the potential of the passive Turbulent Jet Ignition concept for improving the thermal efficiency while decreasing pollutant emissions in SI engines for passenger car applications.

A new fast pre-chamber geometry pre-design methodology based on 1D modelling has been fully developed and experimentally validated. This methodology is original, and the results obtained after its application are of great quality according to the results shown in the paper. The key geometrical parameters of the pre-chamber design have been also identified using this method. Increasing the exchange surface between the pre-chamber and the main chamber by enlarging the diameter of the orifices, favours the filling of the chamber. This lead to an increased Δp between both chambers (main and pre-chamber) that enhances the jet features and therefore the ignition of the main chamber. However, special attention must be paid when increasing the holes diameter excessively due to the loss of fuel mass into the main chamber caused by the increment of pressure during the pre-chamber combustion. From the point of view of the pre-chamber volume, small volumes allow to pressurize the pre-chamber easily, thereby increasing the Δp but compromising the amount of fuel available for the pre-chamber combustion.

The compatibility of this advanced ignition concept with three of the most promising strategies currently under evaluation in the field of SI engines, increasing compression ratio, increasing lambda and dilution with EGR is critically evaluated. The underlying reasons of the observed trends are discussed in detail and cause-effect relations are well established. In this way, performance of the a priori worse pre-chamber design (denoted as pre-chamber 2) is lower than pre-chamber 1 (expected to offer a better performance). Therefore, the hypothesis provided by the model have been confirmed, demonstrating the utility and robustness of the method for pre-design tasks. In addition, advantage was also taken from the numerical model to further understand the experimental trends.

Experiments have also shown that a favourable pre-chamber design allows to extend the ignition limit towards higher air-to fuel ratios. However, it is not possible to achieve $\lambda = 2$ conditions where the amount the generated nitrogen oxides are below the limits established

by the public institutions. Further discussion on this regard suggests that this λ constraint is a consequence of the laminar flame speed reduction but it is also aggravated by the residual gases from the previous cycle that are not evacuated from pre-chamber during the scavenge.

Furthermore, the Turbulent Jet Ignition concept tends to reduce the combustion duration by promoting a faster combustion in the main chamber. This allows to optimize the combustion phasing, therefore improving the indicated efficiency. Both aspects make the Turbulent Jet Ignition concept especially attractive when combined with those strategies that in the search of higher efficiency are very limited by knock (high compression ratio, intake boosting, etc.). Moreover, the combustion deterioration, fundamentally in terms of phasing, significantly conditions efficiency levels as the air-to-fuel ratio increases above 1.2.

It has been shown that the Turbulent Jet Ignition concept is less tolerant to dilution with exhaust gas recirculation than with air. While the maximum air dilution is around 60%, the maximum dilution ratio for exhaust gases is close to 20%. With the help of numerical methods and assuming some reasonable hypotheses, it has been qualitatively proven that the exhaust gases dilution causes combustion to shift to more unstable regimes in the Borghi-Peters diagram, basically due to the effect of a decreased laminar flame velocity and increased flame thickness. Besides, the inherent internal combustion products present in the pre-chamber increases the overall burned gases dilution, hampering the spreading of the exhaust gases dilution range.

In sum, these conclusions highlight the potential advantages and main drawbacks of the Turbulent Jet Ignition concept for the automotive applications. However, some questions related to the phenomena that occurred within the pre-chamber remain unsolved. Further efforts should therefore be taken to further develop the Turbulent Jet Ignition concept though more sophisticated measurement techniques like Particle Image Velocimetry (PIV) and/or numerical methods such as Computational Fluid Dynamics (CFD).

Acknowledgements

The work has been partially supported by the Spanish Ministerio de Economía y Competitividad through Grant No. TRA2017-89139-C2-1-R.

The authors want to express their gratitude to CONVERGENT SCIENCE Inc. and Convergent Science GmbH for their kind support for the 1D calculations with the CONVERGE software.

The authors also wish to thank Mr. Gabriel Alcantarilla for his inestimable assistance during the experimental campaign.

References

[1] Vressner A, Gabrielsson P, Gekas I, Senar-Serra E. Meeting the EURO VI NOx emission legislation using a EURO IV base engine and a SCR/ASC/DOC/DPF configuration in the world harmonized transient cycle. https://doi.org/10.4271/2010-01-1216.

[2] Heywood JB. Internal combustion engine fundamentals. New York: Mcgraw-Hill; 1988.

[3] Attard WP, Konidaris S, Hamori F, Toulson E, Watson HC. Compression ratio effects on performance, efficiency, emissions and combustion in a carbureted and PFI small engine. In: Asia Pacific automotive engineering conference. SAE International; 2007. https://doi.org/10.4271/2007-01-3623.

[4] Attard WP, Parsons P. Flame kernel development for a spark initiated pre-chamber combustion system capable of high load, high efficiency and near zero NOx emissions. SAE Int J Eng 2010;3(2):408–27. https://doi.org/10.4271/2010-01-2260.

[5] Wang J, Chen H, Hu Z, Yao M, Li Y. A review on the pd-based three-way catalyst. Catal Rev 2015;57(1):79–144. https://doi.org/10.1080/01614940.2014.977059. http://www.tandfonline.com/doi/abs/10.1080/01614940.2014.977059.

[6] Germane GJ, Wood CG, Hess CC. Lean combustion in spark-ignited internal combustion engines – a review. In: SAE international fall fuels and lubricants meeting and exhibition. SAE International 1983; 1983. https://doi.org/10.4271/831694.

[7] Attard WP, Blaxill H. A lean burn gasoline fueled pre-chamber jet ignition combustion system achieving high efficiency and low NOx at part load. In: SAE 2012 world congress & exhibition. SAE International; 2012. https://doi.org/10.4271/2012-01-1146.

[8] Yeo G, Kil J, Youn Y, Kim C, Kim N. Three-way catalysts for partial lean-burn engine vehicle. Soc Automotive Eng Korea 2000.

[9] Takami A, Takemoto T, Ichikawa S, Saito F, Komatsu K. Three way catalyst for advanced lean burn engine. In: JSAE spring conference. Society of Automotive Engineers of Japan; 1994.

[10] Peterson B, Reuss DL, Sick V. On the ignition and flame development in a spray-guided direct-injection spark-ignition engine. Combust Flame 2014;161(1):240–55. https://doi.org/10.1016/j.combustflame.2013.08.019. http://www.sciencedirect.com/science/article/pii/S0010218013003234.

[11] Gentz G, Thelen B, Gholamisheeri M, Litke P, Brown A, Hoke J, et al. A study of the influence of orifice diameter on a turbulent jet ignition system through combustion visualization and performance characterization in a rapid compression machine. Appl Therm Eng 2015;81:399–411. https://doi.org/10.1016/j.applthermaleng.2015.02.026. http://www.sciencedirect.com/science/article/pii/S1359431115001349.

[12] Li T, Yin T, Wang B. Anatomy of the cooled EGR effects on soot emission reduction in boosted spark-ignited direct-injection engines. Appl Energy 2017;190:43–56. https://doi.org/10.1016/j.apenergy.2016.12.105. http://www.sciencedirect.com/science/article/pii/S0306261916318773.

[13] Wei H, Zhu T, Shu G, Tan L, Wang Y. Gasoline engine exhaust gas recirculation – a review. Appl Energy 2012;99:534–44. https://doi.org/10.1016/j.apenergy.2012.05.011. http://www.sciencedirect.com/science/article/pii/S0306261912003595.

[14] Galloni E, Fontana G, Palmaccio R. Effects of exhaust gas recycle in a downsized gasoline engine. Appl Energy 2013;105:99–107. https://doi.org/10.1016/j.apenergy.2012.12.046. http://www.sciencedirect.com/science/article/pii/S0306261912009373.

[15] Toulson E, Schock HJ, Attard WP. A review of pre-chamber initiated jet ignition combustion systems. In: SAE 2010 powertrains fuels & lubricants meeting. SAE International; 2010. https://doi.org/10.4271/2010-01-2263.

[16] Alvarez CEC, Couto GE, Roso VR, Thiriet AB, Valle RM. A review of prechamber ignition systems as lean combustion technology for Si engines. Appl Therm Eng 2018;128:107–20. https://doi.org/10.1016/j.applthermaleng.2017.08.118. http://www.sciencedirect.com/science/article/pii/S1359431117302284.

[17] Heyne S, Meier M, Imbert B, Favrat D. Experimental investigation of prechamber autoignition in a natural gas engine for cogeneration. Fuel 2009;88(3):547–52. https://doi.org/10.1016/j.fuel.2008.09.032. http://www.sciencedirect.com/science/article/pii/S0016236108003712.

[18] Attard WP, Bassett M, Parsons P, Blaxill H. A new combustion system achieving high drive cycle fuel economy improvements in a modern vehicle powertrain. In: SAE 2011 world congress & exhibition. SAE International; 2011. https://doi.org/10.4271/2011-01-0664.

[19] Gentz G, Thelen B, Litke P, Hoke J, Toulson E. Combustion visualization, performance, and CFD modeling of a pre-chamber turbulent jet ignition system in a rapid compression machine. SAE Int J Eng 2015;8(2):538–46. https://doi.org/10.4271/2015-01-0779.

[20] Gentz G, Gholamisheeri M, Toulson E. A study of a turbulent jet ignition system fueled with iso-octane: pressure trace analysis and combustion visualization. Appl Energy 2017;189:385–94. https://doi.org/10.1016/j.apenergy.2016.12.055. http://www.sciencedirect.com/science/article/pii/S0306261916318189.

[21] Chinnathambi P, Bunce M, Cruff L. RANS based multidimensional modeling of an ultra-lean burn pre-chamber combustion system with auxiliary liquid gasoline injection April 2015. https://doi.org/10.4271/2015-01-0386. http://papers.sae.org/2015-01-0386/.

[22] Biswas S, Tanvir S, Wang H, Qiao L. On ignition mechanisms of premixed CH4/air and H2/air using a hot turbulent jet generated by pre-chamber combustion. Appl Therm Eng 2016;106:925–37. https://doi.org/10.1016/j.applthermaleng.2016.06.070. http://www.sciencedirect.com/science/article/pii/S135943111630984X.

[23] Allison P, de Oliveira M, Giusti A, Mastorakos E. Pre-chamber ignition mechanism: experiments and simulations on turbulent jet flame structure. Fuel 2018;230:274–81. https://doi.org/10.1016/j.fuel.2018.05.005. http://www.sciencedirect.com/science/article/pii/S0016236118308287.

[24] Biswas S, Qiao L. Ignition of ultra-lean premixed H2/air using multiple hot turbulent jets generated by pre-chamber combustion. Appl Therm Eng 2018;132:102–14. https://doi.org/10.1016/j.applthermaleng.2017.11.073. http://www.sciencedirect.com/science/article/pii/S1359431117353000.

[25] Attard WP, Blaxill H. A single fuel pre-chamber jet ignition powertrain achieving high load, high efficiency and near zero NOx emissions. SAE Int J Eng 2011;5(3):734–46. https://doi.org/10.4271/2011-01-2023.

[26] Attard WP, Blaxill H, Anderson EK, Litke P. Knock limit extension with a gasoline fueled pre-chamber jet igniter in a modern vehicle powertrain. SAE Int J Eng 2012;5(3):1201–15. https://doi.org/10.4271/2012-01-1143.

[27] Attard WP, Toulson E, Huisjen A, Chen X, Zhu G, Schock H. Spark ignition and pre-chamber turbulent jet ignition combustion visualization. In: SAE 2012 world congress & exhibition. SAE International; 2012. https://doi.org/10.4271/2012-01-0823.

[28] Attard WP, Fraser N, Parsons P, Toulson E. A turbulent jet ignition pre-chamber combustion system for large fuel economy improvements in a modern vehicle powertrain. SAE Int J Eng 2010;3(2):20–37. https://doi.org/10.4271/2010-01-1457.

[29] Vedula RT, Gentz G, Stuecken T, Toulson E, Schock H. Lean burn combustion of iso-octane in a rapid compression machine using dual mode turbulent jet ignition system (mar 2018) https://doi.org/10.4271/03-11-01-0007.

[30] Spicher U, Heidenreich T. 2- stratified-charge combustion in direct injection gasoline engines. Zhao H, editor. Advanced direct injection combustion engine technologies and development, vol. 1. Woodhead Publishing; 2010. p. 20–44. https://doi.org/10.1533/9781845697327.20.

[31] Sens M, Binder E. Pre-chamber ignition as a key technology for future powertrain fleets. MTZ Worldwide 2019;80(2):44–51. https://doi.org/10.1007/s38313-018-

0150-1.
[32] Xu G, Kotzagianni M, Kyrtatos P, Wright YM, Boulouchos K. Experimental and numerical investigations of the unscavenged prechamber combustion in a rapid compression and expansion machine under engine-like conditions. Combust Flame 2019;204:68–84. https://doi.org/10.1016/j.combustflame.2019.01.025. http://www.sciencedirect.com/science/article/pii/S0010218019300434.
[33] Wang N, Liu J, Chang WL, fon Lee C. A numerical study of the combustion and jet characteristics of a hydrogen fueled turbulent hot-jet ignition (THJI) chamber. Int J Hydrogen Energy 2018;43(45):21102–13. https://doi.org/10.1016/j.ijhydene.2018.09.156.
[34] Biswas S, Tanvir S, Wang H, Qiao L. On ignition mechanisms of premixed CH4/air and H2/air using a hot turbulent jet generated by pre-chamber combustion. Appl Therm Eng 2016;106:925–37. https://doi.org/10.1016/j.applthermaleng.2016.06.070.
[35] Attard WP, Parsons P. A normally aspirated spark initiated combustion system capable of high load, high efficiency and near zero NOx emissions in a modern vehicle powertrain. SAE Int J Eng 2010;3(2):269–87. https://doi.org/10.4271/2010-01-2196.
[36] Lapuerta M, Armas O, Hernández J. Diagnosis of di diesel combustion from in-cylinder pressure signal by estimation of mean thermodynamic properties of the gas. Appl Therm Eng 1999;19(5):513–29. https://doi.org/10.1016/S1359-4311(98)00075-1. http://www.sciencedirect.com/science/article/pii/S1359431198000751.
[37] Payri F, Molina S, Martín J, Armas O. Influence of measurement errors and estimated parameters on combustion diagnosis. Appl Therm Eng 2006;26(2):226–36. https://doi.org/10.1016/j.applthermaleng.2005.05.006. http://www.sciencedirect.com/science/article/pii/S1359431105001560.
[38] Galindo J, Climent H, Plá B, Jiménez V. Correlations for Wiebe function parameters for combustion simulation in two-stroke small engines. Appl Therm Eng 2011;31(6):1190–9. https://doi.org/10.1016/j.applthermaleng.2010.12.020. http://www.sciencedirect.com/science/article/pii/S1359431110005363.
[39] Bunce M, Blaxill H, Kulatilaka W, Jiang N. The effects of turbulent jet characteristics on engine performance using a pre-chamber combustor. In: SAE 2014 world congress & exhibition. SAE International; 2014. https://doi.org/10.4271/2014-01-1195.
[40] Murase E, Ono S, Hanada K, Oppenheim AK. Pulsed combustion jet ignition in lean mixtures. In: International fuels & lubricants meeting & exposition. SAE International; 1994. https://doi.org/10.4271/942048.
[41] Kalghatgi G, Golombok M, Snowdon P. Fuel effects on knock, heat release and “cars” temperatures in a spark ignition engine. Combust Sci Technol 1995;110(1):209–28.
[42] Borghi R. On the structure and morphology of turbulent premixed flames. Recent advances in the aerospace sciences. Springer; 1985. p. 117–38.
[43] Peters N. The turbulent burning velocity for large-scale and small-scale turbulence. J Fluid Mech 1999;384:107–32.
[44] Mounam¨-Rousselle C, Landry L, Halter F, Foucher F. Experimental characteristics of turbulent premixed flame in a boosted spark-ignition engine. Proc Combust Inst 2013;34(2):2941–9. https://doi.org/10.1016/j.proci.2012.09.008.
[45] Iacovano C, d’Adamo A, Cantore G. Analysis and simulation of non-flamelet turbulent combustion in a research optical engine. Energy Procedia 2018;148:463–70. https://doi.org/10.1016/j.egypro.2018.08.121.
[46] Peters N. Turbulent combustion. Cambridge University Press; 2000.
[47] Convergent Science Inc., Converge 2.3 Theory Manual; 2017.